

31 **1. Introduction**

32 Sudden stratospheric warming (SSW) is large-scale meteorological process in the polar stratosphere
33 which is characterized by rapid rise in temperatures and deceleration/reversal in the zonal mean flows
34 (Scherhag, 1952). The primary driver of SSW is thought to be a rapid growth of quasi-stationary planetary
35 wave interacting with zonal mean flow (Matsuno, 1971). Although the main processes of SSW occur in the
36 middle atmosphere, its effects on the ionosphere have been observed in significant changes of equatorial
37 electrojet (EEJ), vertical plasma drift, and equatorial ionization anomaly (EIA) (Vineeth et al., 2007; Chau
38 et al., 2009; Goncharenko et al., 2010; Pancheva and Mukhtarov, 2011; Jin et al., 2012). These ionospheric
39 variations mainly display similar semidiurnal pattern and 13- to 16-day wave signatures which have been
40 associated with planetary wave, solar and lunar tide wave (Pedatella and Forbes, 2009; Goncharenko et al.,
41 2010; Fejer et al., 2010; Park et al., 2012). Since stationary planetary waves in the Southern Hemisphere
42 (SH) generally have smaller amplitudes than in the Northern Hemisphere (NH) where orographic and
43 thermal forcing is stronger (Andrews et al., 1987), major SSWs often occur in NH. Therefore, most studies
44 about SSW effects on the ionosphere are during NH SSW period.

45 In August to September 2002, three minor SSWs and a major SSW appeared in SH (Varotsos 2002;
46 Baldwin et al., 2003). There is sufficient evidence that a series of unusual atmospheric states occurred in
47 this period, i.e., planetary wave scale quasi 10-day variation (Krüger et al., 2005; Palo et al., 2005),
48 short-term semidiurnal tide variability with zonal wave number $s=1$ (Chang et al., 2009) and the winds
49 oscillation with ~14-days period (Andrew et al., 2004), are all linked to the extremely large planetary wave
50 events. Although the atmospheric activity in connection with 2002 SH SSW has been well revealed in
51 observations and numerical modeling, relatively little is known about the ionosphere effects of 2002 SH
52 SSW. Recently, Olson et al. (2013) studied the equatorial electrodynamic perturbations in Peruvian sector
53 during 2002 SH SSW and found enhanced quasi 2-day fluctuations and large amplitude multi-day
54 perturbations in EEJ and vertical drifts. The researches of ionospheric behavior during SH SSW periods are
55 useful for verifying the existing explanation about the origin of ionospheric perturbations during NH SSW
56 periods and revealing some newer features of ionospheric variation, so further investigation of 2002 SH
57 SSW effect on ionosphere with more ionospheric parameters is still warranted.

58 In the present study, we present the first observational evidence of quasi 10-day oscillation in EIA
59 region during 2002 SH SSW which has not been reported during NH SSWs, based on the location of EIA
60 crests derived from Global Positioning System (GPS) station observations, the Total Electron Content

61 (TEC) obtained by International GNSS Service (IGS) global ionospheric TEC map (GIMs), and the EEJ
62 estimated by geomagnetic field in Asian sector.

63

64 2. Data and Methods

65 The location of EIA crests derived from GPS observations are used to analyze the variation in EIA
66 region during 2002 SH SSW from July 20, 2002 to October 27, 2002. The GPS stations are GUAN
67 (23.19°N, 113.34°E, MLAT~12.52°N) and BAKO (6.49°S, 106.84°E, MLAT~17.18°S) which are near
68 northern and southern EIA crest, respectively. The locations of the GPS stations are shown in Figures 1.
69 Since the ionospheric vertical TEC usually reach the maximum at EIA crest, the location of EIA crest can
70 be obtained by vertical TEC values at each ionospheric penetration point (IPP), which is the intersection of
71 the line of sight and the ionospheric shell (assumed to be 400 km) (Mo et al., 2014). The relative accuracy
72 of the TEC is 0.02 total electron content unit (1TECU= 10^{16} el m⁻²) (Hofmann-Wellenhof et al., 1992). The
73 sample rate of these GPS stations were 30s, so the resolution of the location of EIA crest is less than 25 km
74 (Mo et al., 2017). Figures 2a and 2b show the daily average geomagnetic latitude (MLAT) of northern and
75 southern EIA crests during 2002 SH SSW.

76 The TEC from GIMs are also used to analyze the variation in EIA region. The GIMs provides maps of
77 TEC obtained from a global network of GPS receivers, which have temporal resolution of 2 hours and
78 spatial resolution of 5° in longitude and 2.5° in latitude (Mannucci et al., 1998). The EIA crest usually
79 reaches its maximum development near 14:00 LT (Huang et al., 1989; Yeh et al., 2001), so the daily
80 average TEC obtained by GIMs at 12~14 LT, $\pm 5^\circ \sim \pm 15^\circ$ MLAT, 100°~150°E every day in Asian sector
81 are used to describe the variation in northern and southern EIA region, the results are shown in Figures 2c
82 and 2d.

83 To demonstrate the dynamical process in EIA region, the EEJ is also used in this study, which can be
84 estimated by the difference between the horizontal component of geomagnetic field at TIR (8.7°N, 77.8°E,
85 MLAT~0.03°N) and VSK (17.68°N, 83.32°E, MLAT~8.56°N) (Rastogi et al., 1990). The results are shown
86 in Figures 2e. In addition, the polar stratospheric temperature (90°S, 10hPa) and zonal mean zonal winds
87 (60°S, 10hPa) obtained from National Centers for Environment Prediction (NCEP) are used to examine the
88 extent of the SSW, the results are shown in Figures 2f and 2g. The background of geomagnetic activity
89 index (Kp) and solar flux index (F10.7) from the websites <http://spidr.ngdc.noaa.gov/> are depicted in
90 Figures 2h and 2i.

91 3. Results and Analysis

92 It can be seen from Figures 2f and 2g that there were three obvious minor SH SSW events around day
93 number 230-260 and a major SH SSW event around day number 263-288 (Olson et al., 2013). Figure 3
94 shows the contour map of polar stratospheric temperature (80°S, 10hPa) obtained from NCEP from July 20,
95 2002 to October 27, 2002. An eastward phase progression of quasi 10-day wave is clearly observed around
96 day number 210-270. With SABER temperature data, Palo et al. (2005) also observed similar disturbance
97 and suggested it consists of an eastward-propagating quasi 10-day wave with zonal wave numbers $s=1$
98 superimposed upon a large stationary planetary wave with $s=1$.

99 Now we examine the impact of this quasi 10-day wave on EIA region. It should be noted the
100 solar/magnetospheric forcing on ionosphere are strong due to 2002 SH SSW event occurring during solar
101 maximum year. To exclude these long period fluctuations in EIA region associated with
102 solar/magnetosphere forcing, the periods longer than 15 days in the MLAT location and TEC of EIA crest,
103 and EEJ are removed. Specifically, these parameters are subtracted from their respective 15-day moving
104 average. The residuals are subjected to Lomb-Scargle (L-S) spectral analysis (Lomb,1976; Scargle, 1982),
105 and the results are shown in Figures 4a, 4b, 4c, 4d, and 4e. The horizontal dashed lines represent the 95%
106 confidence level. It is evident that the MLAT location and TEC of EIA crest, and EEJ all exhibit significant
107 quasi 10-day periodic component, which exceed or approach 95% confidence level, suggesting that the
108 whole dynamical process in EIA region is modulated by quasi 10-day wave. Figures 4f and 4g show the
109 L-S spectral analysis of Kp and F10.7. It can be seen that spectral component of Kp also has quasi 10-day
110 periodic component which will be related to solar wind high-speed streams (Lei et al., 2008). However, this
111 quasi 10-day periodic component is too weak to be identified in F10.7, indicating that variation in the solar
112 flux cannot account for this quasi 10-day oscillation in EIA region.

113 To investigate the time evolution of quasi 10-day periodic variation, the Morlet wavelet spectral
114 analysis is applied to MLAT location and TEC of EIA crest, EEJ and Kp which exhibit quasi 10-day
115 oscillation. The periods longer than 15 days in the MLAT location and TEC of EIA crest, and EEJ are
116 removed before the wavelet spectra is generated, and the results are illustrated in Figures 5a, 5b, 5c, 5d, and
117 5e. The black solid contours in each panel indicate a significance level higher than 95%. The white line in
118 each panel represents the cone of influence of the wavelet analysis. The color bar number is the power
119 strength for each parameter. Obviously, the most predominant periodic component in the MLAT location
120 and TEC of EIA crest, and EEJ are quasi 10-day period, which mainly appeared around day number

121 210-290, indicating quasi 10-day oscillations in EIA region go through three minor SSWs and a major
122 SSW period. The time evolution of the power in MLAT location and TEC of northern EIA crest match well
123 those of southern EIA crest, respectively. In addition, we note both the MLAT location and the TEC of EIA
124 crest show the quasi 2-day oscillations during major SSW period (around day number 260-270), which are
125 also found on equatorial ionospheric electric fields and currents at the same period (Olson et al., 2013).
126 Figure 5f shows the wavelet spectral analysis of Kp index. It can be seen that quasi 10-day periodic
127 component is nearly absent in Kp around day number 230-290, suggesting that magnetic activity should not
128 be the driving force for this quasi 10-day oscillation in EIA region.

129 In order to demonstrate the phase relationship of the quasi 10-day oscillations between northern and
130 southern EIA crests, the band-pass filter is performed on the MLAT location and TEC of EIA crest. The
131 absolute values of the MLAT location of EIA crest are used. The band-pass filter is centered at the period of
132 10-day, with half-power points at 8-day and 12-day, and the results are shown in Figure 6. The quasi 10-day
133 wave amplitudes of northern and southern EIA crests are roughly equivalent, which exceed 1.7 degree for
134 MLAT location and 7 TECU for TEC, respectively. Although the quasi 10-day wave of northern EIA crest
135 match well those of southern EIA crest, the wave of northern EIA crest seemed to delay behind southern
136 EIA crest, especially for MLAT location. To further verify this, Figure 7 shows the cross-correlation of
137 quasi 10-day waves in MLAT location (a) and TEC (b) between northern and southern EIA crests. The
138 cross-correlation coefficients of MLAT location and TEC reach 0.8 and 0.93, respectively. Moreover, the
139 maximum cross-correlation coefficients for MLAT location is at 1 day, indicating that the wave of northern
140 EIA crest delay 1 day behind southern EIA crest. This phase difference between northern and southern EIA
141 crests may be due to differences in longitude between two GPS stations.

142

143 4. Discussions

144 In recent years a series of reports have focused on ionospheric perturbations during SSW event. The
145 most predominant features in ionosphere associated with SSW event are semidiurnal pattern and 13- to
146 16-day wave variations, which are attributed to nonlinear interaction of planetary wave, solar and lunar tide
147 wave (Pedatella and Forbes, 2009;Goncharenko et al., 2010; Fejer et al., 2010;Park et al., 2012). As major
148 SSW often occurs in NH, most studies about SSW effects on the ionosphere are during NH SSW period. In
149 August to September 2002, the first major SSW was observed in SH. The NH and SH SSW occurred in
150 Arctic and Antarctic winter, respectively, so the occurring time and location of SH SSW are opposite to

151 those of NH SSW. The researches of ionospheric behavior during SH SSW periods are useful for testing
152 the general rule of ionospheric perturbations during NH SSW periods. For example, Olson et al. (2013)
153 demonstrated that multi-day ionospheric perturbations responding to 2002 SH SSW resemble those
154 observed during NH SSWs and these ionospheric perturbations were associated with enhanced lunar tidal
155 effects.

156 In the current study we present observations of quasi 10-day oscillation in EIA region during the 2002
157 SH SSW that have not been reported during NH SSWs. This quasi 10-day oscillation is absent and weak in
158 Kp and F10.7 index, indicating that the magnetic activity and solar flux cannot account for this quasi
159 10-day oscillation in EIA region. Meanwhile, an unusual atmospheric state occurred in this period that the
160 ozone hole over the Antarctic has a smaller size and splits into two separate holes (Varotsos 2002; Baldwin
161 et al., 2003). This phenomenon is thought to be due to high temperatures the Antarctic, which was
162 contributed to by upward propagation of a planetary wave (Venkat Ratnam et al., 2004). Moreover, strong
163 planetary wave scale quasi 10-day variation was observed in polar stratospheric temperature during this
164 period (Krüger et al., 2005; Palo et al., 2005), so the quasi 10-day oscillations in EIA region may be related
165 to atmosphere perturbations linking the SSW in the Southern Hemisphere.

166 A series of studies have showed how the quasi 10-day planetary wave in stratosphere can penetrate
167 into the ionosphere E region. Krüger et al. (2005) revealed the eastward-traveling waves with periods near
168 10 days and their interaction with quasi-stationary planetary waves forced in the troposphere during 2002
169 SH SSW event, supporting the observational and numerical evidence that the eastward traveling wave
170 interacts with the stationary wave to produce a quasi-periodic amplitude modulation of the stationary waves
171 (Hirota et al., 1990; Ushimaru and Tanaka, 1992). Palo et al. (2005) found an eastward-propagating quasi
172 10-day wave with zonal wave numbers $s=1$ and $s=2$, and a quasi-stationary planetary waves with $s=1$
173 extend from the lower stratosphere to the 100-120 km height region with little amplitude attenuation. While
174 the quasi-stationary planetary wave is confined to the high latitude atmosphere and cannot directly
175 propagate to equatorial ionosphere, the tides were introduced into planetary wave modulation mechanism.
176 Eswaraiyah et al. (2018) reported that zonal diurnal and semidiurnal tide amplitudes in Antarctica
177 mesosphere and lower thermosphere were enhanced around day number 230-290 during 2002 SH SSW,
178 which coincides with the enhanced period of quasi 10-day oscillations in EIA region shown in Figure 5.
179 Moreover, Chang et al. (2009) showed that the short-term variability of the $s=1$ semidiurnal tide is strongly
180 dependent upon the PW1 events (quasi-10-day wave) prior to the major warming during 2002 SH SSW,

181 supporting the suggestion that the quasi-stationary planetary wave can influence migrating and
182 nonmigrating solar tides globally (Liu et al., 2010; Pedatella and Forbes, 2010). So the interactions between
183 quasi-10-day planetary wave and tide will modify the ionosphere E-region winds, which can produce
184 E-region electric fields via the E-region dynamo process. In this study, the evidence of quasi 10-day
185 periodic variation of EIA crests and EEJ strongly supports the suggestion that quasi-10-day planetary wave
186 produced oscillation in EIA region through modulating E-region electric fields. Specifically, the E-region
187 electric fields map to F-region along the magnetic field lines and generate an eastward electric field
188 (Goncharenko, 2010). At the magnetic equator, the eastward electric field with quasi 10-day periodic
189 variation change electron density distribution in the low-latitude region via $\bar{E} \times \bar{B}$ drift, and finally leads to
190 quasi 10-day planetary waves characteristic variations in EIA region. The effects of planetary wave on the
191 equatorial fountain effect have been revealed by the evidence that the vertical and latitudinal structures of
192 the 6-day oscillation in the F region ionosphere peak on both sides of the equator in the EIA region (Gu et
193 al., 2014). The synchronous 10-day oscillation between northern and southern EIA crest in our results are
194 consistent with these observations.

195 In our prior studies, a 14- to 15-day wave during several NH SSW events is ascribed to lunar tide
196 (Mo et al., 2018). So the source of quasi 10-day oscillations in EIA region during 2002 SH SSW is different
197 from 14- to 15-day waves during NH SSW. Moreover, no obvious 14- to 15-day oscillation is found in EIA
198 region during 2002 SH SSW, which may be that the equatorial lunar semidiurnal effects during
199 September-October are weaker than that during January-February (Stening et al., 2011; Pedatella, 2014).
200 Olson et al. (2013) also reported that the perturbations amplitude of EEJ and vertical drifts modulated by
201 lunar semidiurnal tides during SH SSW are smaller than those during NH SSW.

202

203 **5. Conclusions**

204 Using the location and TEC of EIA crests derived from GPS station observations and GIMs, we found
205 a quasi 10-day periodic variability in northern and southern EIA region in Asian sector during the SH SSW
206 of 2002. In the same time period, this quasi 10-day oscillation is also seen in the polar stratospheric
207 temperature and EEJ, which is absent and weak in Kp and F10.7 index, respectively. Previous studies have
208 shown that a strong quasi 10-day planetary wave with zonal wave numbers $s=1$ extend from the lower
209 stratosphere to mesosphere and lower thermosphere (Palo et al., 2005), so the quasi 10-day variation in EIA
210 region should be ascribed to enhanced 10-day planetary wave in lower atmosphere associated with SSW.

211 **Acknowledgements:** The GPS data were from the Crustal Movement Observation Network of China (via
212 e-mail to yglyang@cma.gov. cn) and IGS (available at <http://sopac.ucsd.edu>). The geomagnetic data at
213 TIR and VSK were from WDC for Geomagnetism, Kyoto (available
214 at <http://wdc.kugi.kyoto-u.ac.jp/hyplt/index.html>). The GIMs were downloaded from the site
215 <ftp://cddis.gsfc.nasa.gov>. This research was jointly supported by the National Natural Science Foundation
216 of China (41464006, 41674157, and 41864006), Guangxi Natural Science Foundation
217 (2016GXNSFAA380132), and Chinese Meridian Project. We gratefully acknowledge National Center for
218 Environmental Prediction (NCEP) for providing public access to stratospheric data (available at
219 <https://www.esrl.noaa.gov/psd/data/reanalysis/>).

220 **References**

- 221 Andrews, D. G., Holton, J. R., and Leovy, C. B.: Middle Atmosphere Dynamics, Academic, San Diego,
222 Calif, 1987.
- 223 Andrew, J. D., Vincent, R. A., Murphy, D. J., Tsutsumi, M., Riggini, D. M., and Jarvis, M. J.: The
224 large-scale dynamics of the mesosphere-lower thermosphere during the Southern Hemisphere
225 stratospheric warming of 2002, *Geophys. Res. Lett.*, 31, L14102, doi:10.1029/2004GL020282, 2004
- 226 Baldwin, M., Hirooka, T., O'Neill, A., and Yoden, S.: major stratospheric warming in the Southern
227 Hemisphere in 2002: Dynamical aspects of the ozone hole split, *SPARC Newsl.*, 20, 24-26, 2003.
- 228 Chang, L. C., Palo, S. E., and Liu, H. -L.: Short-term variation of the s=1 nonmigrating semidiurnal tide
229 during the 2002 stratospheric sudden warming, *J. Geophys. Res.*, 114, D03109,
230 doi:10.1029/2008JD010886, 2009.
- 231 Chau, J. L., Fejer, B. G., and Goncharenko, L. P.: Quiet variability of equatorial $E \times B$ drift during a
232 sudden stratospheric warming event. *Geophys. Res. Lett.*, 36,
233 L05101, <https://doi.org/10.1029/2008GL036785>, 2009.
- 234 Eswaraiah, S., Kim, Y. H., Lee, J., Ratnam, M. V., and Rao, S. V. B.: Effect of Southern Hemisphere
235 sudden stratospheric warmings on Antarctica mesospheric tides: First observational study. *J. Geophys.*
236 *Res. Space Physics*, 123, 2127–2140, <https://doi.org/10.1002/2017JA024839>, 2018.
- 237 Fejer, B. G., Olson, M. E., Chau, J. L., Stolle, C., Lühr, H., Goncharenko, L. P., Yumoto, K., and
238 Nagatsuma, T.: Lunar-dependent equatorial ionospheric electrodynamic effects during sudden
239 stratospheric warmings, *J. Geophys. Res.*, 115, A00G03, doi:10.1029/2010JA015273, 2010.
- 240 Goncharenko L. P., Chau, J. L., Liu, H. -L., and Coster, A. J.: Unexpected connections between the

241 stratosphere and ionosphere, *Geophys. Res. Lett.*, 37, L10101, doi:10.1029/2010GL043125, 2010.

242 Gu, S.-Y., Liu, H.-L., Li, T., Dou, X., Wu, Q., and Russell III, J. M.: Observation of the neutral-ion
243 coupling through 6 day planetary wave, *J. Geophys. Res. Space Physics*, 119, 10,376–10,383,
244 doi:10.1002/2014JA020530, 2014.

245 Hirota, I., Kuroi, K., and Shiotani, M.: Midwinter warmings in the Southern Hemisphere stratosphere in
246 1988, *Q. J. R. Meteorol., Soc.*, 116, 929-941, 1990.

247 Hofmann - Wellenhof, B., Lichtenegger, H., and Collins, J.: *GPS—Theory and Practice*, Springer, New
248 York, 1992.

249 Huang, Y. N., Cheng, K., and Chen, S. W.: On the equatorial anomaly of the ionospheric total electron
250 content near the northern anomaly crest region, *J. Geophys. Res.*, 94(A10), 13,515–13,525, 1989.

251 Jin, H., Miyoshi, Y., Pancheva, D., Mukhtarov, P., Fujiwara, H., and Shinagawa, H.: Response of the
252 migrating tides to the stratospheric sudden warming in 2009 and their effects on the ionosphere studied
253 by a whole atmosphere-ionosphere model GAIA with COSMIC and TIMED/SABER observations, *J.*
254 *Geophys. Res.*, 117, A10323, doi:10.1029/2012JA017650, 2012.

255 Krüger, K., Naujokat, B., and Labitzke, K.: The unusual midwinter warming in the Southern Hemisphere
256 stratosphere 2002: A comparison to Northern Hemisphere phenomena, *J. Atmos. Sci.*, 62, 603-613,
257 2005.

258 Lei, J., Thayer, J. P., Forbes, J. M., Wu, Q., She, C., Wan, W., and Wang, W.: Ionosphere response to solar
259 wind high-speed streams, *Geophys. Res. Lett.*, 35, L19105, doi:10.1029/2008GL035208, 2008.

260 Liu, H. -L, Wang, W., Richmond, A. D., and Roble, R. G.: Ionospheric variability due to planetary waves
261 and tides for solar minimum conditions, *J. Geophys. Res.*, 115, A00G01, doi:10.1029/2009JA015188,
262 2010.

263 Lomb, N. R.: Least-squares frequency analysis of unequally spaced data, *Astrophys.Space Sci.*, 39,
264 447-462, 1976.

265 Mannucci, A. J., Wilson, B. D., Yuan, D. N., Ho, C. M., Lindqwister, U. J., and Runge, T. F.: A global
266 mapping technique for GPS derived ionospheric total electron content measurements, *Radio Sci.*, 33,
267 565-582, doi:10.1029/97RS02707, 1998.

268 Matsuno, T.: A dynamical model of the stratospheric sudden warming, *J. Atmos. Sci.*, 28, 1479-1494, 1971.

269 Mo, X. H., Zhang, D. H., Goncharenko, L. R., Hao, Y. Q., and Xiao, Z.: Quasi-16-day periodic meridional
270 movement of the equatorial ionization anomaly, *Ann. Geophys.*, 32, 121-131, 2014.

271 Mo, X. H., Zhang, D. H., Goncharenko, L. R., Zhang, S. R., Hao, Y. Q., Xiao, Z., Pei, J. Z., Yoshikawa, A.,
 272 Chau, H. D.: Meridional movement of northern and southern equatorial ionization anomaly crests in the
 273 East-Asian sector during 2002–2003 SSW, *Science China Earth Sciences*, 60(4), 776–785, [https://](https://doi.org/10.1007/s11430-016-0096-y)
 274 doi.org/10.1007/s11430-016-0096-y, 2017.

275 Mo, X. H., and Zhang, D. H.: Lunar tidal modulation of periodic meridional movement of equatorial
 276 ionization anomaly crest during sudden stratospheric warming, *J. Geophys. Res. Space Physics*, 123,
 277 1488-1499. <https://doi.org/10.1002/2017JA024718>, 2018.

278 Olson, M. E., Fejer, B. G., Stolle, C., Lühr, H., and Chau, J. L.: Equatorial ionospheric electrodynamic
 279 perturbations during Southern Hemisphere stratospheric warming events, *J. Geophys. Res. Space*
 280 *Physics*, 118, 1190-1195, doi:10.1002/jgra.50142, 2013.

281 Palo, S. E., Forbes, J. M., Zhang, X., Russell III, J. M., Mertens, C. J., Mlynczak, M. G., Burns, G. B., Espy,
 282 P. J., and Kawahara, T. D.: Planetary wave coupling from the stratosphere to the thermosphere during the
 283 2002 Southern Hemisphere pre-stratwam period, *Geophys. Res. Lett.*, 32, L23809,
 284 doi:10.1029/2005GL024298, 2005.

285 Pancheva, D., and Mukhtarov, P.: Stratospheric warmings: The atmosphere-ionosphere coupling paradigm, *J.*
 286 *Atmos. Sol. Terr. Phys.*, 73, 1697-1702, doi:10.1016/j.jastp.2011.03.006, 2011.

287 Park, J., Lühr, H., Kunze, M., Fejer, B. G., and Min, K. W.: Effect of sudden stratospheric warming on
 288 lunar tidal modulation of the equatorial electrojet, *J. Geophys. Res.*, 117, A03306,
 289 doi:10.1029/2011JA017351, 2012.

290 Pedatella, N. M., and Forbes, J. M.: Modulation of the equatorial F-region by the quasi-16 day planetary
 291 wave, *Geophys. Res. Lett.*, 34, L09105, doi:10.1029/2009GL037809, 2009.

292 Pedatella, N. M., and Forbes, J. M.: Evidence for stratosphere sudden warming-ionosphere coupling due to
 293 vertically propagating tides, *Geophys. Res. Lett.*, 37, L11104, doi:10.1029/2010GL043560, 2010.

294 Pedatella, N. M.: Observations and simulations of the ionospheric lunar tide: Seasonal variability, *J.*
 295 *Geophys. Res. Space Physics*, 119, 5800-5806, doi:10.1002/2014JA020189, 2014.

296 Rastogi, R. G., and Klobuchar, J. A. : Ionospheric electron content within the equatorial F2 layer anomaly
 297 belt, *J. Geophys. Res.*, 95(A11), 19,045–19,052, <https://doi.org/10.1029/JA095iA11p19045>, 1990.

298 Scargle, J. D.: Studies in astronomical time series analysis. II. Statistical aspects of spectral analysis of
 299 unevenly spaced data, *Astrophys. J.*, 263, 835-853, 1982.

300 Scherhag, R.: Die explosionsartigen Stratosphärenwärmungen des Spätwinters 1952, *Ber. Dtsch*

301 Wetterdienstes USZone, 6, 51-63, 1952.

302 Stening, R. J.: Lunar tide in the equatorial electrojet in relation to stratospheric warmings, *J. Geophys. Res.*,
303 116, A12315, doi:10.1029/2011JA017047, 2011.

304 Ushimaru, S., and Tanaka, H.: A numerical study of the interaction between stationary Rossby waves and
305 eastward-traveling waves in the Southern Hemisphere stratosphere, *J. Atmos., Sci.*, 49, 1354-1373,
306 1992.

307 Varotsos, C.: The Southern Hemisphere ozone hole split in 2002, *Environ. Sci. Pollut. Res.*, 9, 375-376,
308 2002.

309 Venkat Ratnam, M., Tsuda, T., Jacobi, C., and Aoyama, Y.: Enhancement of gravity wave activity observed
310 during a major Southern Hemisphere stratospheric warming by CHAMP/GPS measurements, *Geophys.*
311 *Res. Lett.*, 31, L16101, doi:10.1029/2004GL019789, 2004.

312 Vineeth, C., Pant, T. K., Devasia, C. V., and Sridharan, R.: Atmosphere-ionosphere coupling observed over
313 the dip equatorial MLTI region through the quasi 16-day wave. *Geophys. Res. Lett.*, 34,
314 L12102, <https://doi.org/10.1029/2007GL030010>, 2007.

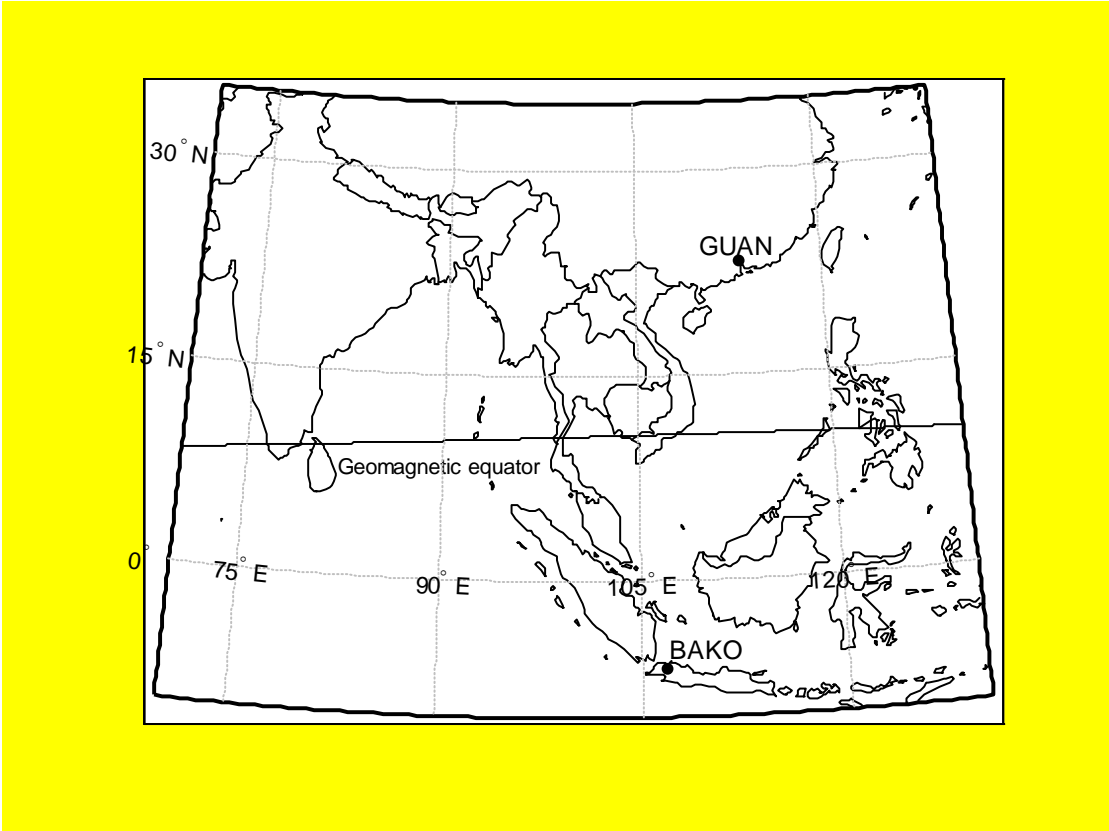
315 Yeh, K. C., Franke, S. J., Andreeva, E. S., and Kunitsyn, V. E.: An investigation of motions of the
316 equatorial anomaly crest, *Geophys. Res. Lett.*, 28(24), 4517-4520, doi:10.1029/2001GL013897, 2001.

317

318

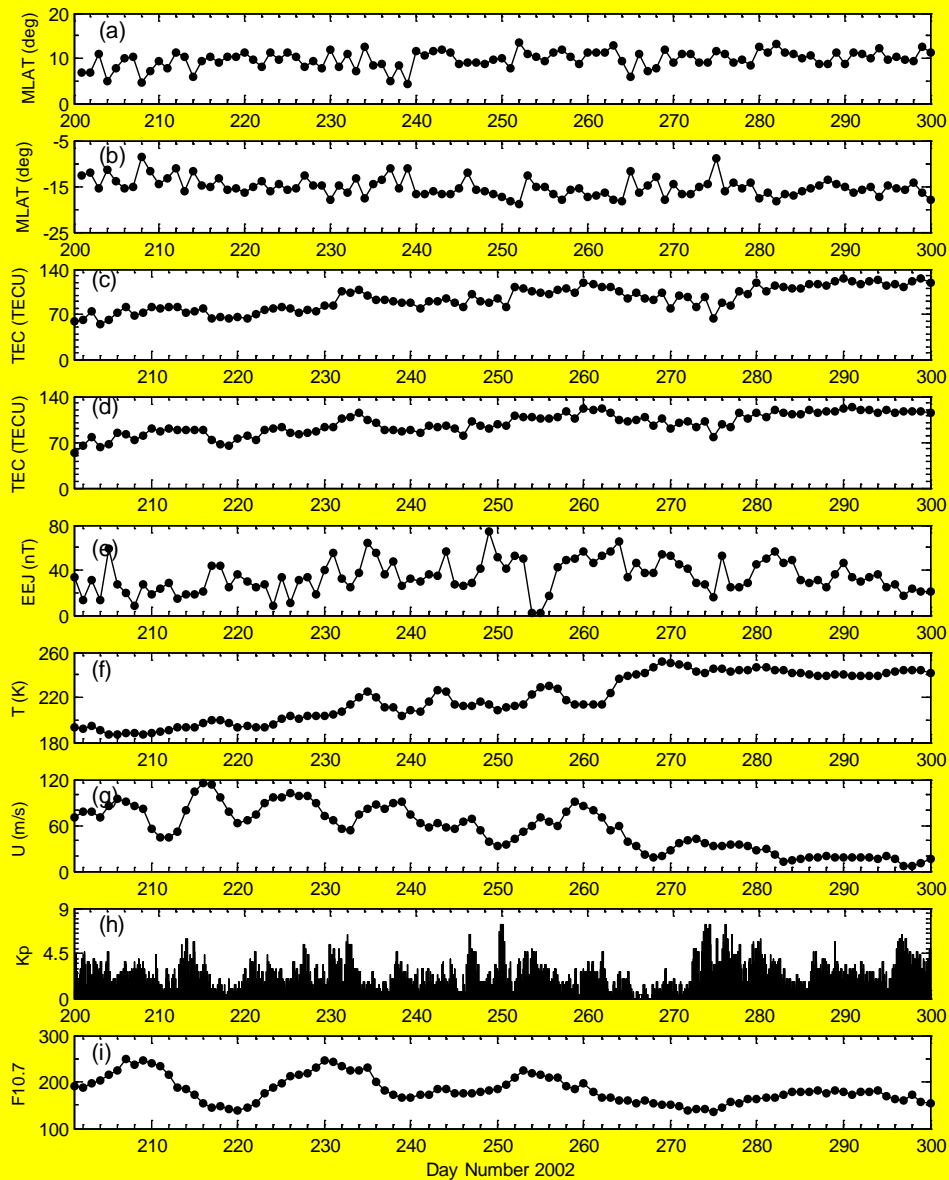
319

320

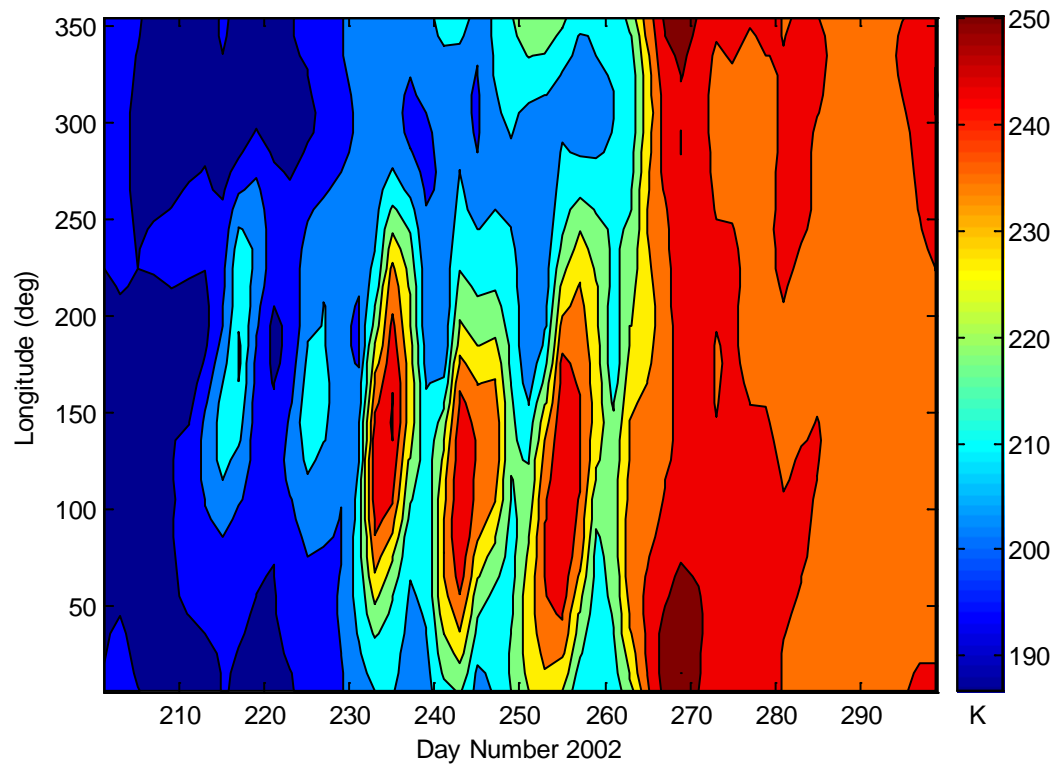


321
322

Figure 1. Location of the GPS stations in Asian sector.



323
 324 **Figure 2.** The magnetic latitude (MLAT) location of (a) northern and (b) southern equatorial ionization
 325 anomaly (EIA) crest; The TEC of (c) northern and (d) southern EIA crest; the (e) equatorial electrojet (EEJ),
 326 (f) polar stratospheric temperature (at 90°S, 10hPa) and (g) zonal wind (at 60°S, 10hPa) from National
 327 Centers for Environment Prediction; the (h) Geomagnetic activity index, Kp and (i) solar flux index F10.7
 328 during the period from July 20, 2002 to October 27, 2002.

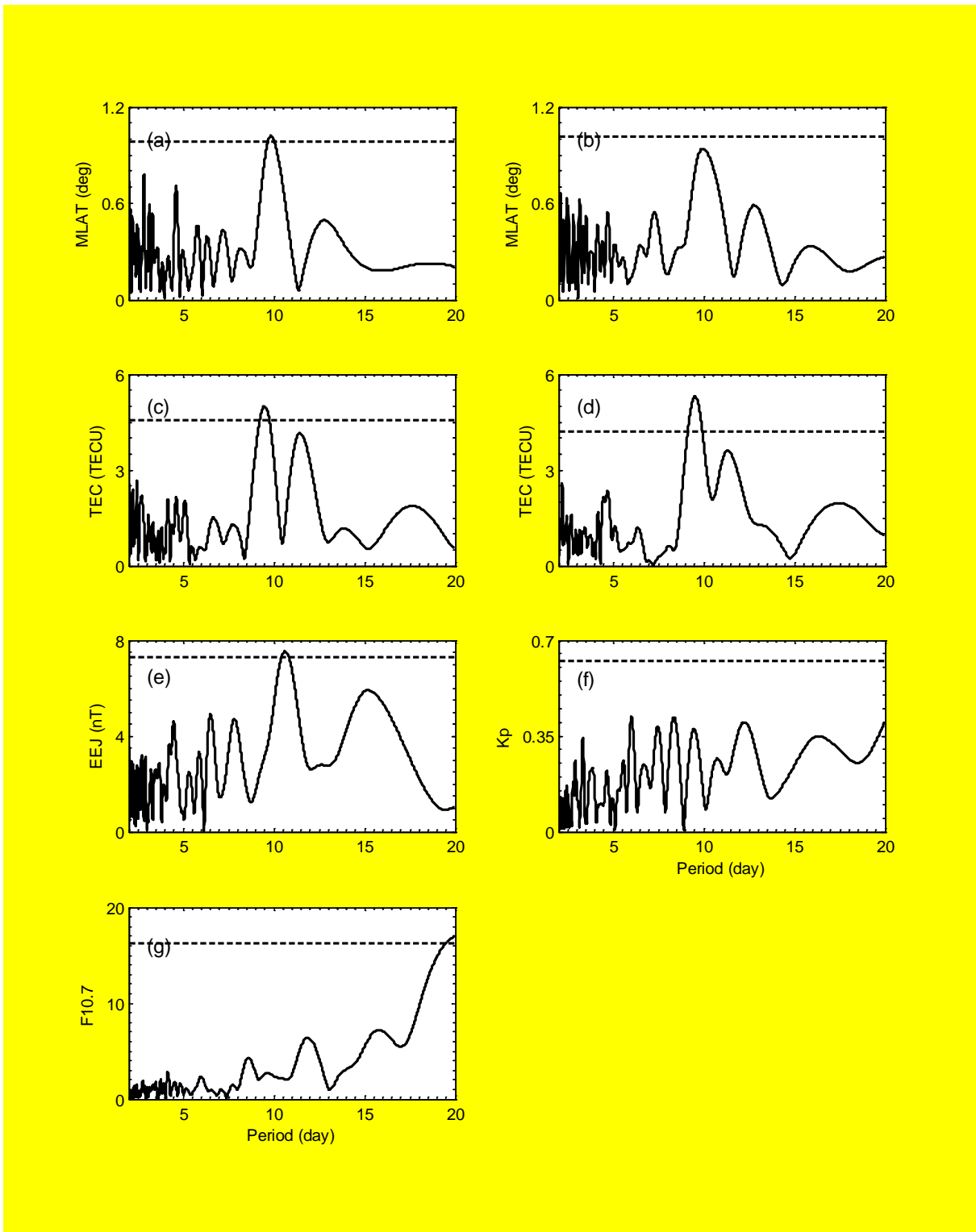


329

330 **Figure 3.** The contour map of polar stratospheric temperature (80°S, 10hPa) obtained from NCEP during

331

the same period as in Figure 2.



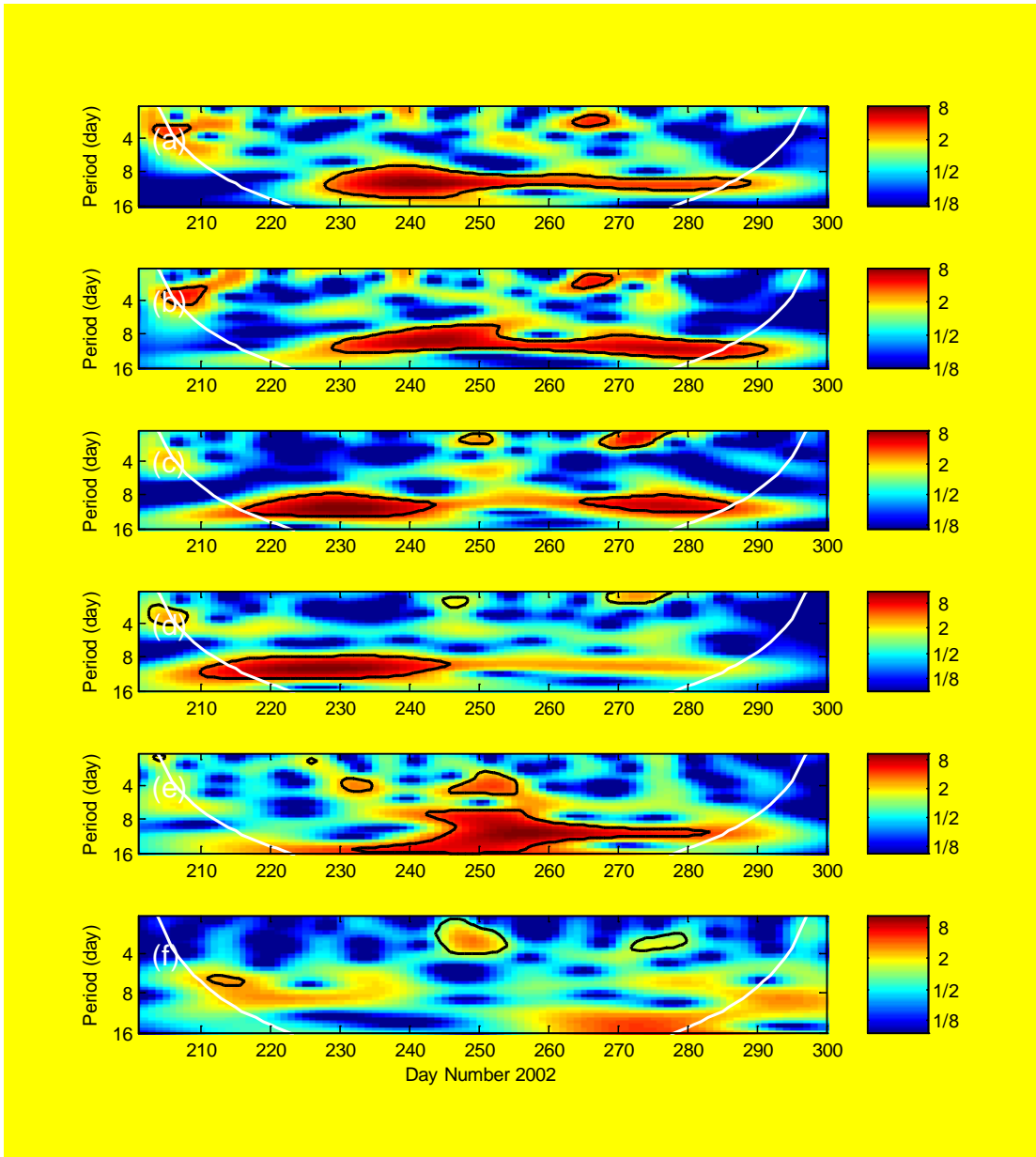
332

333

334

335

Figure 4. Lomb-Scargle periodograms of the MLAT location of (a) northern and (b) southern EIA crest, the TEC of (c) northern and (d) southern EIA crest, (e) EEJ, (f) Kp index and (g) F10.7 during the same period as in Figure 2.

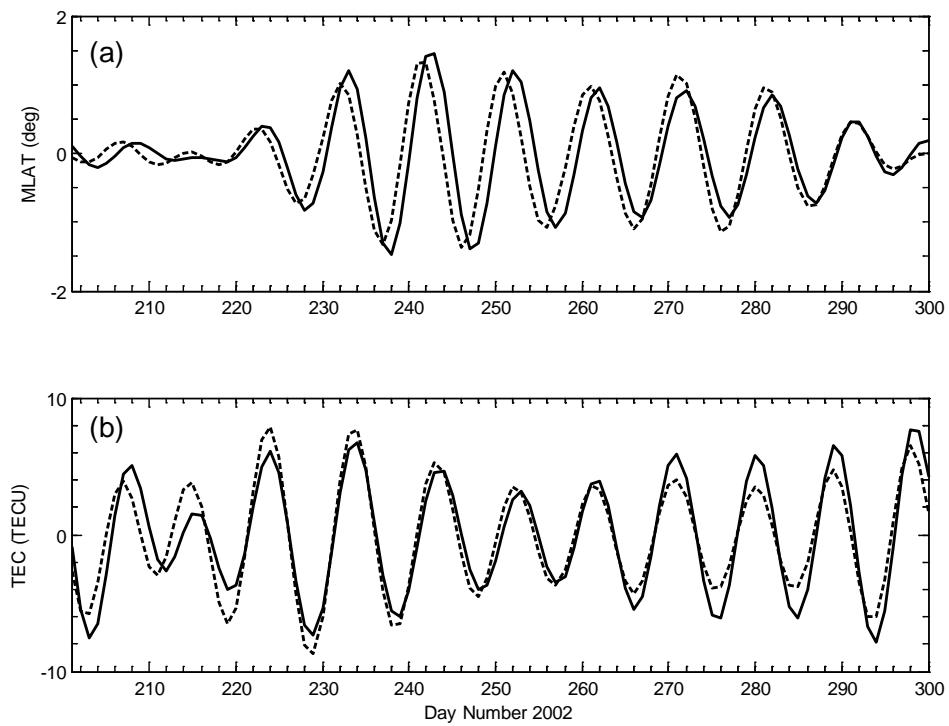


336

337 **Figure 5.** The wavelet power spectra of the MLAT location of (a) northern and (b) southern EIA crest, the

338 TEC of (c) northern and (d) southern EIA crest, (e) EEJ and (f) Kp index during the same period as in

339 Figure 2. The white line in each panel represents the cone of influence of the wavelet analysis.



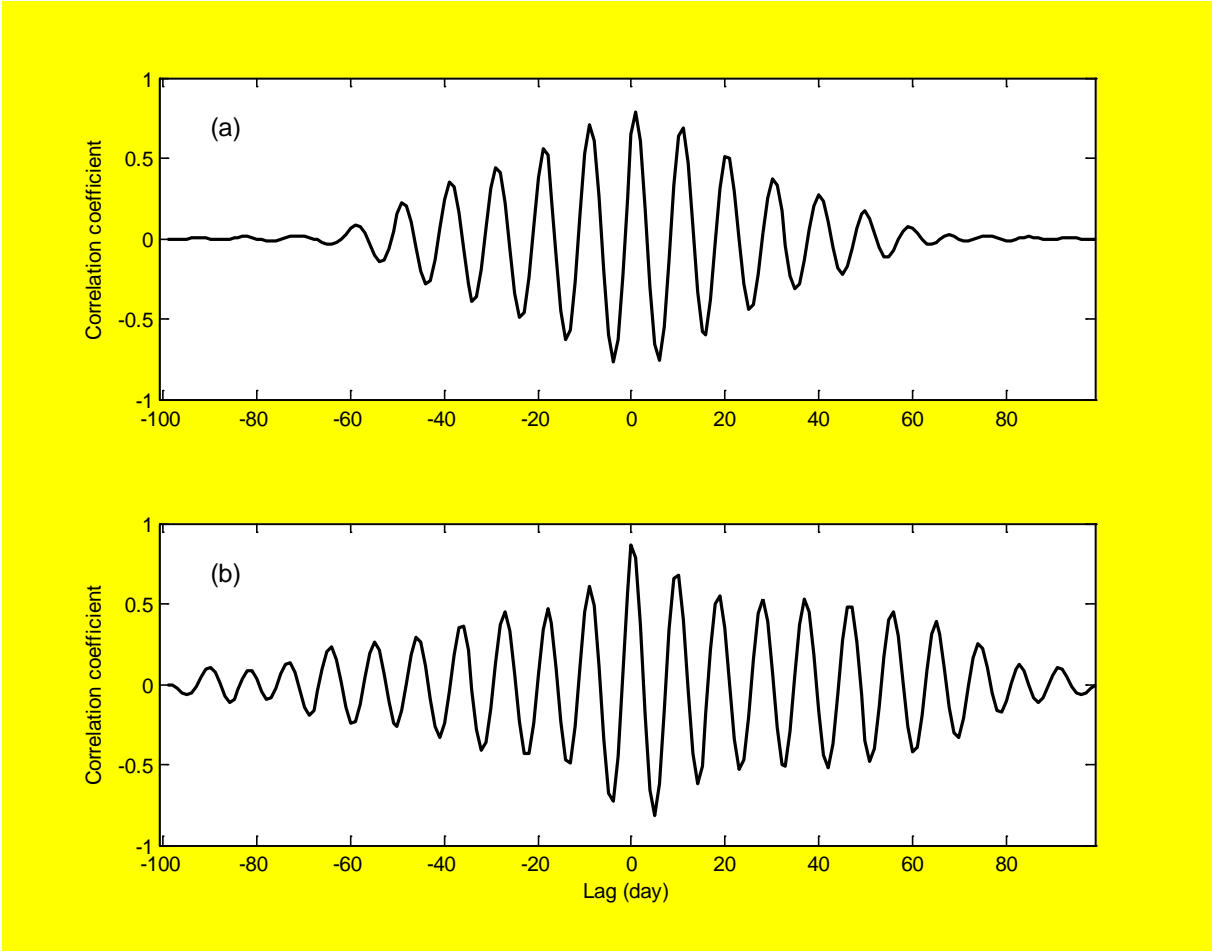
340

341 **Figure 6.** The band-pass filter results of the (a) MLAT location of (solid line) northern and (dash-dotted

342 line) southern EIA crest, the (b) TEC of (solid line) northern and (dash-dotted line) southern EIA crest

343

during the same period as in Figure 2.



344

345 **Figure 7.** The cross-correlation of quasi 10-day waves in MLAT location (a) and TEC (b) between northern

346

and southern EIA crest.